Cerebral Cortex, February 2017;27: 903–918

doi: 10.1093/cercor/bhx003
Advance Access Publication Date: 24 January 2017
Original Article

ORIGINAL ARTICLE

Heparan Sulfates Support Pyramidal Cell Excitability, Synaptic Plasticity, and Context Discrimination

Daniel Minge[1], Oleg Senkov[2], Rahul Kaushik[2], Michel K. Herde[1], Olga Tikhobrazova[3,4], Andreas B. Wulff[1], Andrey Mironov[4,5], Toin H. van Kuppevelt[6], Arie Oosterhof[6], Gaga Kochlamazashvili[3,7], Alexander Dityatev[2,3,4,8] and Christian Henneberger[1,9,10]

[1]Institute of Cellular Neurosciences, University of Bonn Medical School, 53105 Bonn, Germany, [2]German Center for Neurodegenerative Diseases (DZNE), 39120 Magdeburg, Germany, [3]Department of Neuroscience and Brain Technologies, Istituto Italiano di Tecnologia, 16163 Genova, Italy, [4]Department of Neurotechnology, Lobachevsky State University of Nizhny Novgorod, 603950 Nizhny Novgorod, Russia, [5]Central Research Laboratory, Nizhny Novgorod State Medical Academy, 603005 Nizhny Novgorod, Russia, [6]Department of Biochemistry, Radboud Institute for Molecular Life Sciences, Radboud University Medical Center, Nijmegen, The Netherlands, [7]Department of Molecular Pharmacology and Cell Biology, Leibniz-Institut für Molekulare Pharmakologie (FMP), 13125 Berlin, Germany, [8]Medizinische Fakultät, Otto-von-Guericke-Universität Magdeburg, 39120 Magdeburg, Germany, [9]German Center for Neurodegenerative Diseases (DZNE), 53175 Bonn, Germany and [10]Institute of Neurology, University College London, London WC1N 3BG, UK

Address correspondence to Christian Henneberger, Institute of Cellular Neurosciences, University of Bonn Medical School, Sigmund-Freud-Str. 25, 53105 Bonn, Germany. Email: christian.henneberger@uni-bonn.de or Alexander Dityatev, German Center for Neurodegenerative Diseases (DZNE), Leipziger Str. 44, 39120 Magdeburg, Germany. Email: alexander.dityatev@dzne.de

D. Minge and O. Senkov have contributed equally to this study.

Abstract

Heparan sulfate (HS) proteoglycans represent a major component of the extracellular matrix and are critical for brain development. However, their function in the mature brain remains to be characterized. Here, acute enzymatic digestion of HS side chains was used to uncover how HSs support hippocampal function in vitro and in vivo. We found that long-term potentiation (LTP) of synaptic transmission at CA3–CA1 Schaffer collateral synapses was impaired after removal of highly sulfated HSs with heparinase 1. This reduction was associated with decreased Ca^{2+} influx during LTP induction, which was the consequence of a reduced excitability of CA1 pyramidal neurons. At the subcellular level, heparinase treatment resulted in reorganization of the distal axon initial segment, as detected by a reduction in ankyrin G expression. In vivo, digestion of HSs impaired context discrimination in a fear conditioning paradigm and oscillatory network activity in the low theta band after fear conditioning. Thus, HSs maintain neuronal excitability and, as a consequence, support synaptic plasticity and learning.

Key words: extracellular matrix, heparan sulfates, learning, neuronal excitability, synaptic plasticity

Introduction

Heparan sulfate proteoglycans (HSPG) are present throughout the brain and are located on cell membranes but also in the extracellular matrix (ECM). HSPGs represent a heterogeneous group of proteins, among them the ECM molecules agrin and perlecan as well as cell surface molecules like syndecans and glypicans (Sarrazin et al. 2011). A common feature of HSPGs is covalently bound side chains of heparan sulfates (HSs), which are often the sites of interactions with ligands such as growth factors (Sarrazin et al. 2011; Matsuo and Kimura-Yoshida 2014).

These HSs are unbranched polysaccharides that are synthesized from *N*-glucuronic acid and *N*-acetylglucosamine before extensive modification by, for instance, sulfation. HSPGs play a well-established role during brain development. They are important for patterning of the brain, neurogenesis and crucial for axonal guidance (Yamaguchi et al. 2010). Consequently, most studies of HSPGs have focused on developmental aspects of HSPG signaling.

In addition, HSPGs can profoundly modulate memory and learning in adult animals and synaptic long-term plasticity in acute slices prepared from these (Senkov et al. 2014). Interestingly, a recent study demonstrated that conditional ablation of Ext1, a gene involved in HS synthesis, from a subpopulation of pyramidal neurons leads to an autistic phenotype (Irie et al. 2012). These findings indicate that HSPGs and HSs shape brain function on many levels from cellular properties to complex behavior.

However, both a developmental phenotype and the acute absence of the HSPGs or HSs may underlie such a deficit in the adult. Acute enzymatic digestion of ECM components has been used to identify specific roles of ECM components and to isolate their acute contribution to adult brain functions (Senkov et al. 2014). For example, enzymatic digestion of hyaluronic acid in intact brain tissue can be achieved within only 2 h (Kochlamazashvili et al. 2010), thus avoiding potential developmental side effects of genetic manipulations. Similar to hyaluronic acid, the function of HSs has been studied mainly by either genetic ablation of the HS bearing proteoglycans or enzymatic digestion of HS side chains. In dissociated hippocampal cultures, enzymatic removal of highly sulfated HSs with heparinase 1 affects synaptic scaling and decreases the mean firing rate of neurons (Korotchenko et al. 2014; Garau et al. 2015). In acute hippocampal slices, treatment with a combination of heparinases 1 and 3, which supposedly removes both low and highly sulfated HSs, impairs long-term potentiation (LTP) of synaptic transmission (Lauri et al. 1999; Dityatev et al. 2004). However, the type of involved HSs and the cellular and network mechanisms underlying this LTP impairment have remained unclear. In addition, it is mostly unknown how HSs acutely affect behavior or network activity in vivo.

Here, we addressed these open questions by a combination of electrophysiological, imaging, and behavioral experiments. Our results in vitro show that removal of highly sulfated HSs reduces CA1 pyramidal cell excitability, which in turn leads to decreased dendritic and spine Ca^{2+} entry and impaired LTP. In vivo, the reduced excitability is associated with altered oscillatory network activity in the low theta range and abolished contextual discrimination in a fear conditioning paradigm.

Materials and Methods

Slice Preparation and Heparinase Treatment

Acute hippocampal slices were prepared from 5 to 8-week-old male C57BL/6 mice and Thy1-YFP (Feng et al. 2000) mice as previously described (Kochlamazashvili et al. 2010; Anders et al. 2014). Briefly, acute hippocampal slices were obtained in full compliance with national and institutional guidelines on animal experimentation. Slices, 350 µm thick unless stated otherwise, were prepared in an ice-cold slicing solution containing (in mM): NaCl 60, sucrose 105, KCl 2.5, $MgCl_2$ 7, NaH_2PO_4 1.25, ascorbic acid 1.3, sodium pyruvate 3, $NaHCO_3$ 26, $CaCl_2$ 0.5, and glucose 10 (osmolarity 300–305 mOsm), and kept in the slicing solution at 34 °C for 15 min before being stored at room temperature (RT, 21–23 °C) in an extracellular solution containing (in mM) NaCl 126, KCl 2.5, $MgSO_4$ 1.3, NaH_2PO_4 1.25, $NaHCO_3$ 26, $CaCl_2$ 2, and glucose 10. This solution was also used for recordings at RT. Heparinase 1 from *Flavobacterium heparinum* (Sigma H2519, 1 U/mL) was used for enzymatic removal of HSs from hippocampal slices in custom-made aerated incubation chambers (2 mL volume, at 34 °C). For sham treatment, a subset of heparinase aliquots was heat-inactivated for 120 min at 60 °C. All solutions were continuously bubbled with 95% O_2/5% CO_2.

In Vitro Electrophysiology

For recordings, hippocampal slices were transferred to a submersion-type recording chamber and superfused with extracellular solution at RT. For extracellular recordings, standard patch pipettes (3–4 MΩ) were filled with extracellular solution and inserted into the CA1 *stratum radiatum*. Whole-cell recordings from CA1 pyramidal cells were obtained using standard patch pipettes (3–4 MΩ) filled with an intracellular solution containing (in mM) KCH_3O_3S 135, HEPES 10, di-Tris-Phosphocreatine 10, $MgCl_2$ 4, Na_2-ATP 4, Na-GTP 0.4 (pH adjusted to 7.2 using KOH, osmolarity 290–295 mOsm). Membrane-impermeable dyes Oregon Green 488 BAPTA-1 (OGB1, 200 µM, Invitrogen), OGB6F (250 µM), Fluo-4 (200 µM), and Alexa Fluor 594 hydrazide (20 µM, Invitrogen) were added to the intracellular solution as indicated. In a subset of recordings, KCH_3O_3S was replaced by equimolar $CsCH_3O_3S$. Data were recorded using MultiClamp 700B amplifiers, digitized (10–40 kHz) and stored for offline analysis. Whole-cell recordings were rejected if at any time the access resistance exceeded 20 MΩ or changed by more than 20%. Bridge balance and series resistance compensation was used as appropriate. For stimulation experiments, a bipolar concentric stimulation electrode was placed in the "stratum radiatum" at the border between CA2/3 and CA1. For theta-burst stimulations (TBS), 8 bursts consisting of 4 stimuli (0.1 ms each, 100 Hz) were delivered at 5 Hz (a single TBS cycle). The pattern was repeated up to 5 times (5x TBS) with an interval of 1 min between individual TBSs. For LTP experiments presented in Figure 1, the stimulation intensity was adjusted to obtain field excitatory postsynaptic potentials (fEPSPs) with a slope of 50% of the subthreshold maximum (subthreshold maximum: fastest-rising fEPSP without a clearly visible population spike in the decay phase) (Kochlamazashvili et al. 2010). For experiments presented in Figures 2 and 4, the stimulus intensity was set to 4 times the intensity needed to elicit a single action potential by a single test burst of 5 stimuli at 100 Hz to compensate for variable stimulation efficiencies between slices (Kochlamazashvili et al. 2010). In some experiments, *N*-methyl-D-aspartate receptor (NMDAR)-mediated fEPSPs were recorded in the presence of 0.1 mM Mg^{2+} and isolated pharmacologically by the α-amino-3-hydroxy-5-methyl-4-isoxazolepropionic acid receptor (AMPAR)-inhibitor NBQX. In these experiments, a cut was made between CA3 and CA1.

Characterization of current clamp data was performed using custom written Matlab (Mathworks) scripts previously described (Heeroma et al. 2009). For analysis of data in Figure 4*e* and Supplementary Figure 6, values were averaged over all 5

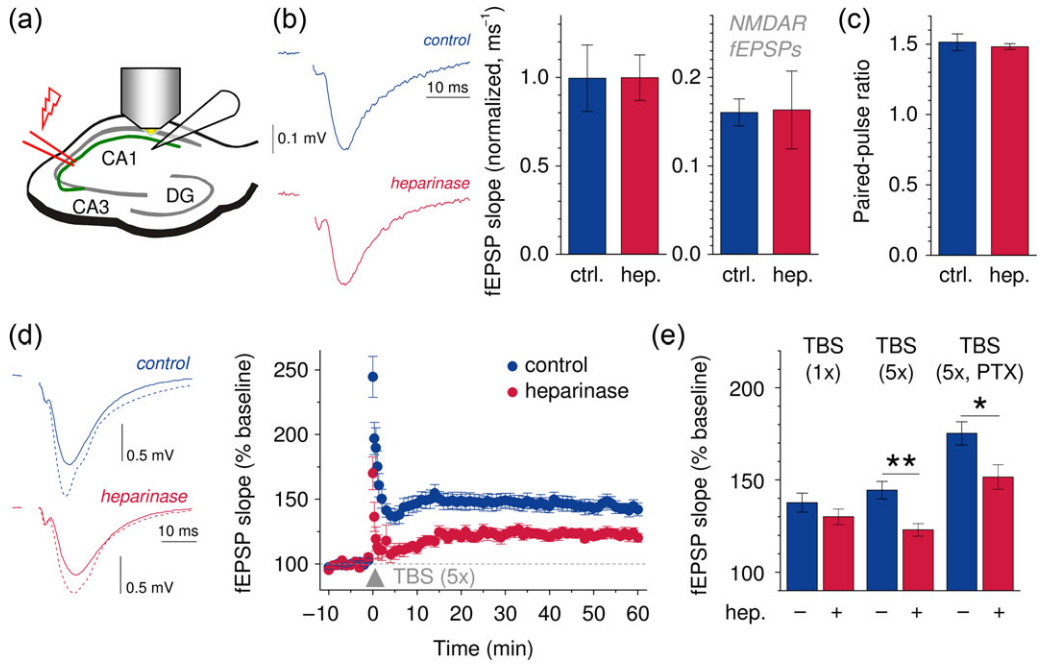

Figure 1. Removal of HSs impairs LTP of synaptic transmission at CA3–CA1 Schaffer collateral synapses in acute hippocampal slices. (*a*, *b*) Schematic recording configuration. fEPSPs were recorded in the stratum radiatum of the CA1 region and evoked by electrical stimulation of CA3–CA1 Schaffer collaterals. Sample fEPSPs recorded from control and heparinase-treated slices (blue and red, respectively, left panel). fEPSP slopes normalized to the axonal fiber volley were virtually indistinguishable between control and heparinase-treated slices ($n = 9$ both groups, middle panel). Stimulation intensity for bar graphs was 100 µA (please see Supplementary Fig. 2*a–c* for the complete range of stimulus intensities tested, fiber volleys and slopes before normalization and statistics). NMDAR-mediated fEPSPs were recorded in the presence of 0.1 mM Mg^{2+} and the AMPAR-inhibitor NBQX and were not significantly different between control and heparinase-treated slices (right panel, $n = 6$ both groups, please see Supplementary Fig. 2*d* for complete range of stimulus intensities and statistics). (*c*) The fEPSP paired-pulse ratio was not different between control and heparinase-treated slices ($n = 9$ both). The interstimulus interval was 50 ms (please see Supplementary Fig. 2*d*,*e* for sample traces, the complete range of intervals tested and statistics). (*d*) LTP was induced by TBS. Sample traces before (solid lines) and after LTP induction (dotted lines) are shown for control- and heparinase-treated slices (left panel, blue and red, respectively). Time courses of fEPSP slopes in LTP experiments are shown in the right panel ($n = 8$ both groups, 5 TBS cycles). (*e*) LTP induced by a single TBS is not affected by removal of HSs (1× TBS, $n = 8$ both groups, $P = 0.267$, unpaired *t*-test). In contrast, strong LTP-inducing stimuli (5 cycles of TBS, $n = 8$ both groups, $P = 0.0024$, unpaired *t*-test) uncovered an LTP deficit in heparinase-treated slices. The effect persisted in the presence of the GABA receptor antagonist PTX (100 µM, $n = 8$ and 7 for control and heparinase-treated slices, $P = 0.023$, unpaired *t*-test).

current injection cycles after 4-way ANOVA had indicated that the cycle is not a significant factor.

Channel or receptor blockers D-AP5 (50 µM, Abcam), NBQX disodium salt (10 µM, Abcam), CGP52432 (5 µM, Abcam), nifedipine (20 µM, Sigma-Aldrich), picrotoxin (PTX, 100 µM, Abcam), and tetrodotoxin (TTX, 1 µM, Tocris) were added to the extracellular solution as indicated.

Immunocytochemistry and Immunohistochemistry

Mouse hippocampal neurons were cultured for 24 days in vitro and incubated with 0.5 U/mL of heparinase 1 for 2 h at 37 °C as described previously with some modifications (Dityatev et al, 2004) and fixed with 4% paraformaldehyde (PFA), permeabilized with 0.1% Triton-X-100 in phosphate-buffered saline (PBS) for 10 min, washed 3 times and blocked (0.1% Glycine + 0.1% Tween-20 + 10% Normal Goat Serum in PBS) for 45 min at RT. Anti-HS antibody A04B08V (dilution 1:2; the antibody was purified against mouse skeletal muscle HS and supposed to recognize 2-O and 6-O high sulfate group) (Dam et al. 2003) diluted in blocking buffer was applied for overnight followed by 3 washes with PBS. Incubation with secondary antibody (anti-VSV-G, clone P5D4, dilution 1:100) and tertiary antibody (Mouse, Alexa 488, dilution 1:1000) was carried out for 3 and 1 h, respectively. Coverslips were subsequently washed with PBS, incubated with DAPI (Invitrogen, reference number-D1306) for 10 min and mounted using fluoromount aqueous mounting media (Sigma-F4680). For hippocampal sections, the similar procedure was applied but permeabilization step was carried out with 0.5% Triton-X-100 in PBS for 10 min and anti-VSV-G, clone P5D4 antibody was used with the dilution 1:50.

For ankyrin G (AnkG) labeling, acute horizontal hippocampal slices (250 µm thick) of three 52–58-day-old Thy1-YFP animals (Feng et al. 2000) were prepared and treated with heparinase as described above. After heparinase/control incubation, the slices were immersion-fixed in 4% PFA in PBS (pH 7.4) at 4 °C for 2 h. Next, slices were washed for 3 × 30 min in PBS before incubation in a blocking solution (5% normal goat serum and 0.1% Triton-X-100 in PBS) at RT for 6 h. Primary antibodies against GFP (host: chicken, 1:5000, Abcam, ab13970) and AnkG (mouse monoclonal, 1:500, Neuromab, clone N106/36) were incubated in blocking solution at 4 °C for 40 h. After a 3 × 30 min PBS wash, secondary antibodies (goat antichicken Alexa Fluor 488, goat antimouse Alexa Fluor 568, both 1:200, Invitrogen) were incubated at RT for 2 h. Slices were again washed 3 × 30 min in PBS before being mounted with ProLong Gold Antifade (Invitrogen). Imaging was performed on a Leica SP8 confocal microscope with a glycerol immersion 63x, 1.3 NA objective and hybrid detectors. Initial image analysis was done by an experimenter blinded to the experimental conditions using ImageJ (NIH) and Microsoft Excel. CA1 pyramidal cell axon initial segments (AISs) were identified using the YFP-label and their typical morphology and confirmed by AnkG labeling. Axonal AnkG expression profiles were obtained from image stacks by average intensity projections of all

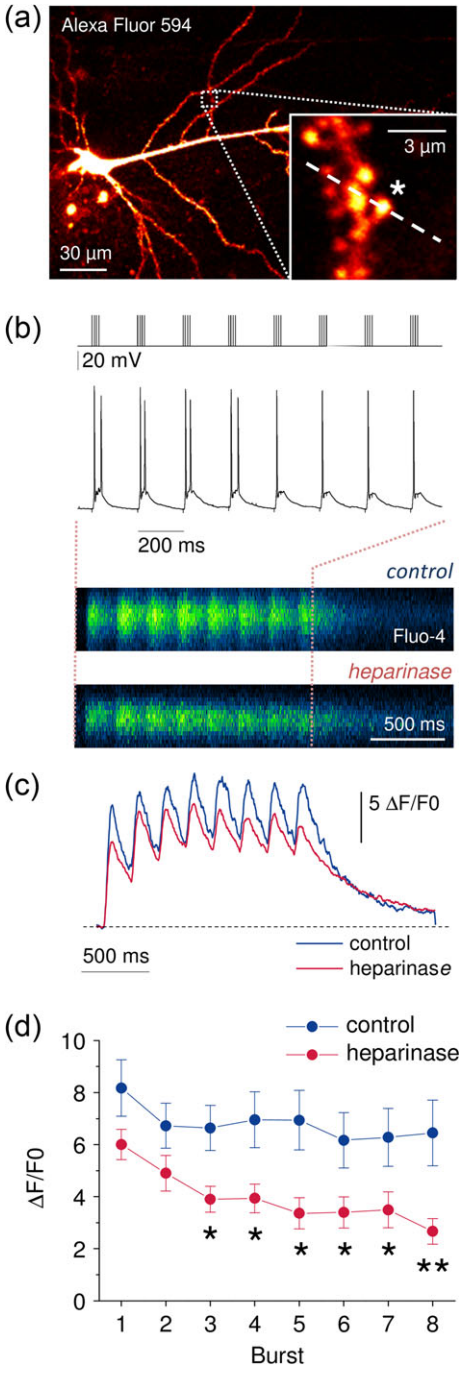

Figure 2. Ca^{2+} entry at spines and dendrites of CA1 pyramidal cells during TBS is reduced in heparinase-treated hippocampal slices. (*a*) CA1 pyramidal cells were held in the whole-cell patch-clamp configuration and filled via the patch pipette with the Ca^{2+}-sensitive fluorescent dye Fluo-4 (200 µM) and the morphological marker Alexa Fluor 594 (20 µM). Dendrites and synaptic spines were visualized using 2PE fluorescence microscopy (excitation wavelength 800 nm). Positions of line scans across dendrites and spines were pseudo-randomly chosen (inset, position of line scan indicated by dashed line, 0.4–0.8 kHz). (*b*) Fluorescence changes were monitored (line scans, *a*) during TBS (top panel, stimulus pattern) while neurons were recorded from in current clamp mode (middle panel). Representative line scans of Fluo-4 fluorescence from sham and heparinase-treated slices are shown in the bottom panel (average of 5 TBS). (*c*) Global averages of Fluo-4 fluorescence traces reveal reduced Ca^{2+} entry in heparinase-treated slices ($n = 10$ and 11 for control and heparinase treatment). (*d*) Ca^{2+} entry was quantified by calculating $\Delta F/F_0$ (see Materials and Methods for details) for each burst and corrected for decaying fluorescence from the previous burst. Lower values of $\Delta F/F_0$ in heparinase-treated cells indicate a reduced Ca^{2+} entry during TBS after removal of HSs (2-way repeated measures ANOVA, $P = 0.021$, unpaired *t*-tests for individual bursts). Illustrated experiments were performed in the presence of AP5 (see text for further details).

imaging planes containing AnkG signal (max stack z-depth 5 µm). A line profile was then drawn along the AIS starting from the center of the soma and finishing just beyond the most distal AnkG signal (typically 40–45 µm from the soma). Further details are provided in Figure 5 and the corresponding Results section.

For AnkG labeling in dissociated cultures, mouse hippocampal cultures were treated with heparinase and heat-inactivated heparinase (control) as described above after 21 days in vitro (DIV21). Subsequently, cells were quickly rinsed with warm PBS and subjected to above-mentioned immunocytochemistry protocol to stain with antibodies against AnkG (mouse monoclonal, 1:1000) and MAP2 (guinea pig, 1:500). Imaging was performed with the experimenter blinded to the experimental groups on a Zeiss LSM 700 confocal microscope with a 63x/1.4 NA oil immersion objective. Image analysis was done using ImageJ (NIH) and Microsoft Excel. AISs were detected as AnkG positive immunofluorescence starting from the edge of the soma as defined by MAP2 positive immunostaining. Of note, 40 µm long fluorescence intensity line profiles were taken along the AIS starting from the edge of the soma.

In Vivo Electrophysiology, Intrahippocampal Injection and Behavioral Testing

Animals

Adult (2–4-month old) male C57BL/6 J mice (Charles River) were used. At least 1 week before start of the experiments, mice were transferred to a small vivarium, where they were housed individually with food and water ad libitum on a reversed 12:12 light/dark cycle (light on at 9:00 PM). All behavioral experiments were performed in the afternoons during the dark phase of the cycle when mice are active, under constant temperature (22 ± 1 °C) and humidity (55 ± 5%). All treatments and behavioral procedures were conducted in accordance with ethical animal research standards defined by German law and approved by the Ethical Committee on Animal Health and Care of the State of Saxony-Anhalt, Germany, the licence number 42502-2-1159 DZNE.

Fabrication of Electrodes and Cannulas

We have used a previously described hybrid infusion-multielectrode (HIME) recording system for acute drug delivery at the place of acquisition of neuronal activity (Senkov et al. 2015). In short, a 5 electrodes bundle was made of tungsten wires insulated with Teflon and bound together in a stainless steel tubing. Electrode tips were arranged to aim to different major hippocampal layers, using a decrement of 250 µm between each electrode, starting from 2 mm length, to reach molecular layer of the dentate gyrus (DG), and ending with the shortest electrode, 1–1.1 mm, to record from *stratum oriens* and *pyramidale*. For fabrication of guide cannulas, we used the same stainless steel tubing as for electrodes.

Implantation of Electrodes and Cannulas

Chronic implantation of electrodes and cannulas in mice was performed as described previously (Kochlamazashvili et al. 2010; Senkov et al. 2015) (see Fig. 7*a* for a schematic of electrode and cannula placement). In brief, mice were anesthetized with

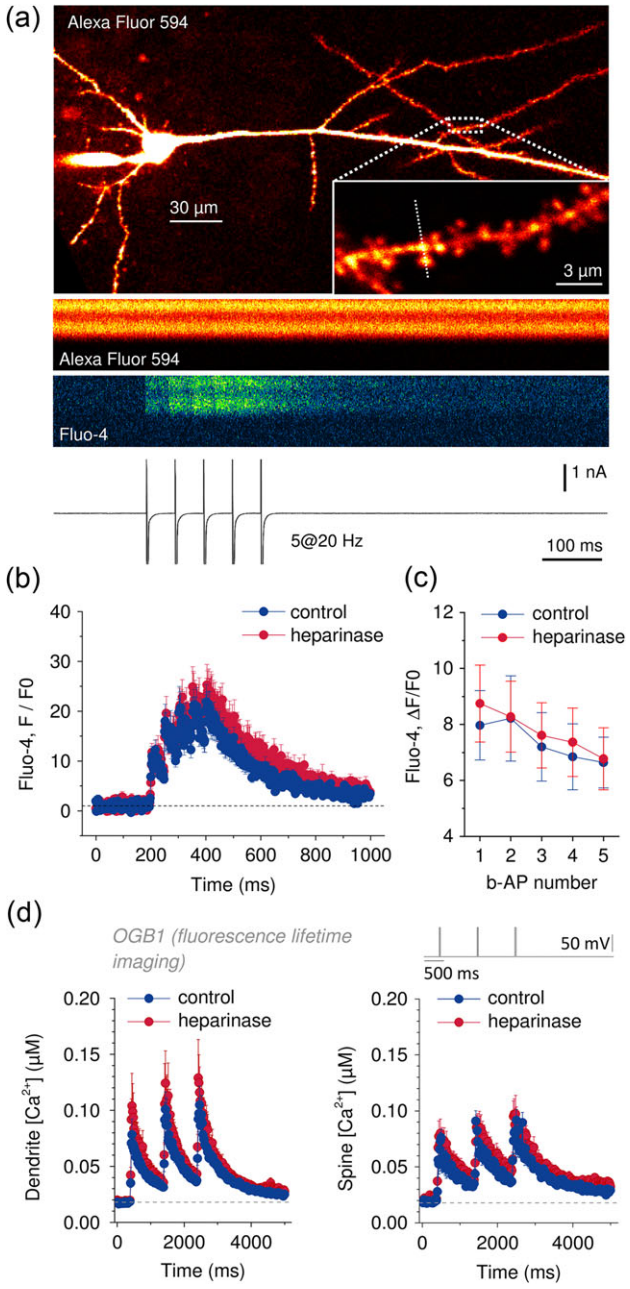

Figure 3. Ca^{2+} entry induced by b-APs or direct depolarization is not affected by heparinase treatment. (*a*) Pyramidal cells were held in whole-cell voltage clamp at −70 mV and filled via the patch pipette with the Ca^{2+}-sensitive fluorescent dye Fluo-4 (200 µM) and the morphological marker Alexa Fluor 594 (20 µM). Dendrites and synaptic spines were visualized using 2PE fluorescence microscopy at 800 nm. Position of line scans across dendrites and spines was pseudo-randomly chosen (inset, position of line scan indicated by dashed line, 0.4–0.8 kHz). b-APs were evoked by brief (2–3 ms) voltage jumps to +10 mV (2–3 ms each, 5 at 20 Hz, sample trace with clipped action currents in bottom panel). Fluo-4 fluorescence line profiles indicate robust Ca^{2+} entry in response to b-APs while Alexa Fluor 594 fluorescence remains stable. (*b*, *c*) Time courses of Fluo-4 fluorescence during b-APs trains in control and heparinase-treated slices. No significant differences could be detected (n = 16 and 25 for sham and heparinase treatment, respectively, 2-way repeated measures ANOVA, P = 0.96). (*d*) Ca^{2+} entry in response to direct, AP-independent depolarization was investigated by FLIM in cells filled with the Ca^{2+}-sensitive fluorescent dye Oregon Green BAPTA-1 (OGB1, 200 µM, please see Supplementary Fig. 3 and text for further details). Ca^{2+} responses were evoked by brief voltage steps from −70 to +20 mV for 25 ms (3× at 1 Hz) in the presence of TTX (1 µM). OGB1 lifetimes were translated into Ca^{2+} concentrations and their time courses were plotted. No significant difference was detected between control and heparinase-treated spines and dendrites (n = 13 for control spines, all other n = 12, amplitudes 2-way repeated measures ANOVA, P = 0.39 for dendrites and 0.55 for spines).

1–3% isoflurane (Baxter International, Inc.). Preparation for implantation included injection and application of analgesics, head hair shaving, and skin cleaning and application of an antiseptic as previously described (Senkov et al. 2015) before the mouse was placed in a stereotaxic frame (Narishige). All following procedures were performed under a surgical binocular microscope and on a heating pad to maintain mouse body temperature constant (34–36 °C) over surgery. A 10 mm diameter circular scalp incision was done and exposed skull bone was cleaned and dried. After marking coordinates for implantation, 3 small holes for anchoring and ground screws were drilled in 2 frontal bones and one in the left parietal at the border with the interparietal bone. Two frontal screws and a parietal screw were connected with a ground/reference wire. The left cannula was stereotactically implanted after drilling another hole and by using a self-made universal holder and fixed using acrylic. Next, hippocampal electrodes were implanted in the right parietal bone. After hippocampal electrodes, the right cannula was similarly implanted and secured with acrylic. Coordinates for bilateral cannulas: AP = 2.0 mm and L = ±2.2 mm from Bregma and midline, respectively. Coordinates for the 5 electrodes bundle reaching different layers of the hippocampus were: AP = −2.0 mm from Bregma and L = ±1.25 mm; DV = 2.0 mm from the brain surface. The whole system was secured to the bone with dental cement and the Neuralynx EIB-16 headstage was screwed into position. Finally, tungsten wire tails from electrodes were gently connected to the headstage. After the assembly was completed, all ground wires were soldered together and the upper cover "hat" as a Faraday cage was placed above the bottom pedestal and fixed to it with 2 small screws. Surgery typically lasted 90 min. Mice were allowed to recover for at least 5–7 days before behavioral test and recordings (postoperative analgesic: carprofen, 5 mg/kg b.w. s.c.).

Intrahippocampal Injection

For intrahippocampal injection, we used a digitally controlled infusion system (UltraMicroPump, UMP3, and Micro4 Controller, WPI) fed with a 10 µL Hamilton syringe and a NanoFil (35 GA) bevelled needle. The mouse was first anesthetized with 1–3% isoflurane and put into the stereotaxic frame. The headstage EIB-16 was then gently unscrewed and shifted to expose underneath electrodes and cannulas. The dummy cannula was gently removed from the left guide cannula before the NanoFil injecting needle was inserted into the guide cannula and active heparinase 1 (0.05 U/1 µL per site, Sigma-Aldrich) or, as control treatment, heat-inactivated heparinase 1 (30 min boiling in 100 °C) was injected at a rate of 3 nL/s. After waiting for another 5 min, the injection needle was replaced by the dummy and the same procedure was performed on the other hemisphere. The duration of the procedure including re-mounting of the headstage after injection was about 25–30 min.

Fear Conditioning

A classical Pavlovian contextual fear conditioning (CFC) paradigm was used. In short, CFC was done at day 0 (d0) as follows: 1 day after intrahippocampal injections, mice were placed in a neutral context (CC–) for 5 min to record behavior and electroencephalography (EEG). 1–2 h later the same mice were placed into a conditioned context (CC+) for 5 min and 3x medium

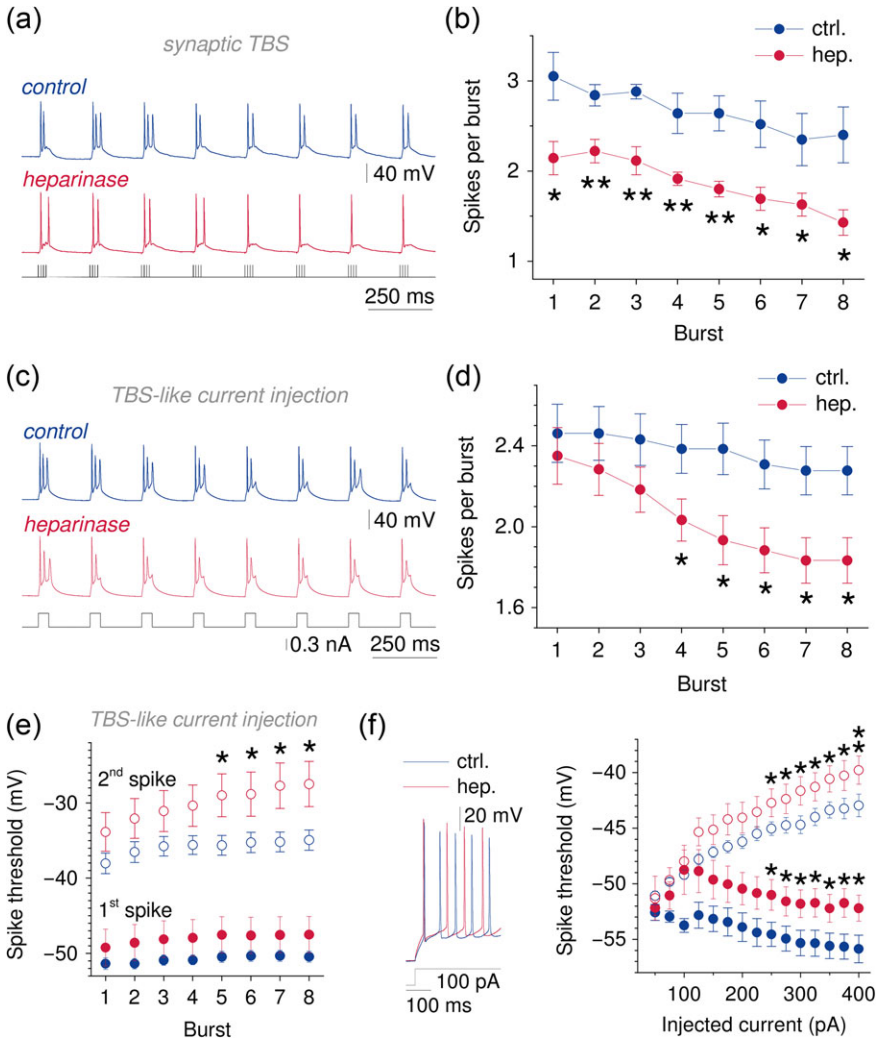

Figure 4. CA1 pyramidal cells generate fewer action potentials during TBS and TBS-like current injections after heparinase treatment. (*a*, *b*) Representative current clamp recordings from CA1 pyramidal cells during synaptic TBS from control (blue, top) and heparinase (red, middle panel) treated slices (stimulation pattern, bottom panel). Note the reduced number of action potentials generated during individual bursts after heparinase treatment. The number of spikes was analyzed for each burst, averaged over 5 TBS cycles and found to be lower in heparinase-treated neurons (2-way repeated measures ANOVA, $P = 0.003$, $n = 5$ for control slices and 7 for heparinase-treated slices). (*c*, *d*) Current injections with a TBS-like pattern (40 ms, 8 times at 5 Hz, 5 cycles as in *a*, *b*) evoked fewer action potentials in CA1 pyramidal cells from heparinase-treated slices (2-way repeated measures ANOVA, $P = 0.040$, $n = 13$ and 12 for control and heparinase-treated slices, unpaired *t*-tests for individual bursts). This suggests that reduced neuronal excitability may underlie deficits of Ca^{2+} influx and LTP. (*e*) The threshold of spikes evoked by TBS-like current injections was progressively increased after heparinase treatment. While no effect was observed on the first spike in each burst (2-way repeated measures ANOVA, $P = 0.239$) the threshold of the second spike was increased during repetitive stimulation (2-way repeated measures ANOVA, $P = 0.031$, unpaired *t*-tests for individual bursts; first and second spike, filled and empty circles; color coding as above, $n = 13$ for control and $n = 13$ and 12 for first spikes and 13 and 10 for second spikes). (*f*) A qualitatively similar increase of spike thresholds was unmasked when spiking was evoked by constant current injections of increasing intensity in the current clamp configuration (same color coding as in *e*, sample traces and current injection left panel, statistics right panel, $n = 10$ for control and 8 for heparinase treatment, 2-way repeated measures ANOVA, $P = 0.043$ and 0.030, unpaired *t*-tests).

intensity foot shocks were applied (0.5 mA, 1 s) with an interval of 1 min. The protocol was 2 min exploration of CC+, then first shock, after 1 min second shock, and again after 1 min the third shock, mice were then given another minute in CC+ before being removed. EEG was not recorded during the training. The conditioned context (CC+) was a chamber (20×20×30 cm) with contrast black-and-white chess-like pattern on the walls and a metal grid on the floor (75% ethanol was used for cleaning). The neutral context (CC–) was the same chamber, but with gray walls and gray plastic floor, and another type of cleaning solution was used with a different smell. On d1 and d3, the mice were subjected to retrieval sessions. First, mice were placed in CC+ for 5 min and then 1–2 h later they were placed into CC– context for 5 min. All tests were recorded with video synchronized with EEG. For CFC, we used a computerized fear conditioning system (Ugo Basile). The behavior of mice during fear conditioning was recorded for offline analysis using an USB video camera and a behavioral video acquisition and analysis software (AnyMaze). All recorded movies were analyzed by a trained observer blinded to the treatment group. Total freezing time was calculated as the percentage of 5 min (in either of the 2 contexts, CC+ and CC–).

LFP Recordings

Intrahippocampal local field potentials (LFPs) were recorded by using a 64 channels recording system and the acquisition

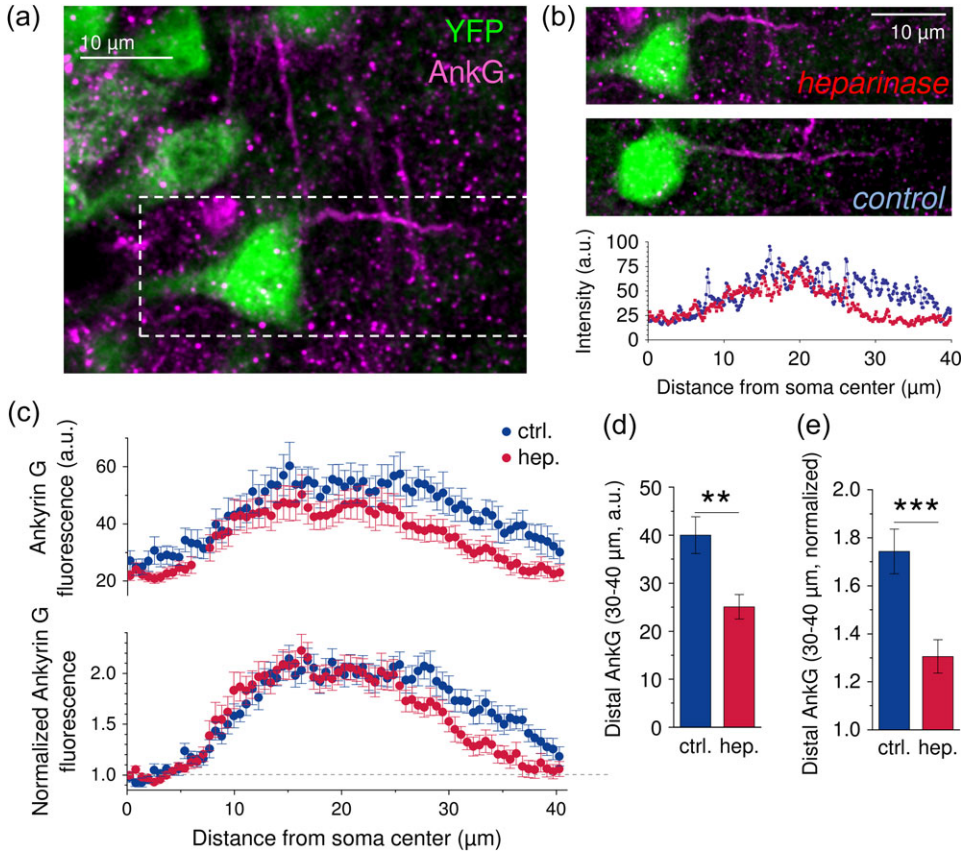

Figure 5. AnkG expression is reduced in the distal AIS after heparinase treatment. (*a*) Mice expressing the fluorescent protein YFP (green) under the Thy1 promoter (Feng et al. 2000) were used to identify CA1 pyramidal cells and their presumptive AISs. The AIS was visualized by colabeling with a mouse anti AnkG antiserum (magenta). (*b*) Sample AnkG labeling of an AIS from a heparinase-treated slice (top panel magnified from *a*, dashed box) and a control slice (middle panel). AnkG labeling in dissociated cultures (see Supplementary Fig. 8 and Results) predicted a distal reduction of ASI AnkG labeling after heparinase treatment. Therefore, the axonal AnkG distribution was determined by taking a line profile (width = 0.57 µm) along the AIS starting from the center of the pyramidal cell soma. The background-corrected AnkG profiles of the examples are shown in the bottom panel (blue control, red heparinase). (*c*) To avoid distorted AnkG profiles due to the large variability of the AIS start (see Results and Supplementary Fig. 9), we selected only axonal AnkG profiles where the AIS started within mean ± 3 × SEM for further analysis. The average fluorescence intensity profiles are shown (n = 17 for control and 21 for heparinase-treated slices). Note that distance is given relative to the soma center in these plots. (*d*) The average background-corrected AnkG signal in the distal AIS (30–40 µm from the soma center) was reduced in heparinase-treated slices (P = 0.0019, unpaired t-test). (*e*) A similar result was obtained when axonal AnkG profiles were normalized to values obtained near the axonal hillock to account for variability of excitation and detection of the fluorescent label (P = 0.00049, unpaired t-test).

software Cheetah (both Neuralynx). LFPs were recorded at 3200 Hz sampling rate, a 0.1–300 Hz wide-band filter, ×1000 amplification, and stored for offline analysis. LFPs were analyzed using NeuroExplorer (5.0, Madison). To record from a freely moving mouse, we used a 5 m cable (Neuralynx) counterbalanced with an equal weight of the headstage and the cable itself. For further data analysis, we chose 2 electrodes targeting 2 most interesting structures (CA1 and DG) involved in contextual memory and contextual discrimination, and electrodes were selected based on following criteria: 1) length of electrodes; 2) histology depicting electrode traces (Fig. 6*b*); 3) lowest theta power is characteristic for CA1 *stratum pyramidale*, whereas highest theta power for molecular layer of DG (Fig. 6*c*); 4) high-frequency oscillations as ripples are characteristic for *stratum pyramidale* and/or *radiatum*.

Two-Photon Excitation (2PE) Ca^{2+} Imaging

CA1 pyramidal cells, their dendrites, and spines were visualized by 2-photon excitation (2PE) fluorescence microscopy. We used a Scientifica system (Scientifica) and a FV10MP imaging system (Olympus) optically linked to a femtosecond pulse laser (Vision S, Coherent, λ = 800 nm) both integrated with patch-clamp electrophysiology (Multiclamp 700B, Molecular Devices) (Kochlamazashvili et al. 2010; Henneberger and Rusakov 2012; Anders et al. 2014). Setups were equipped with 25× (NA 1.05) and 40× (NA 0.8) objectives (Olympus). The laser power was adjusted for depth in the tissue to obtain, on average, 2–3 mW in the focal plane. Fluorescent dyes were loaded via the whole-cell patch-clamp pipette. Once in whole-cell mode, Alexa Fluor 594 typically equilibrated across the neuron within 10–15 min and was used to visualize dendrites and spines. For fluorescence recordings from spines and dendrites, a region of interest was pseudo-randomly chosen. Rapid scans across a line covering spines and dendrites were performed (line scans, 0.4–0.8 kHz) synchronized to electrophysiology. After background correction, fluorescence intensity (F) or its changes (ΔF) were normalized to the baseline fluorescence (F_0) before any stimulus to obtain F/F_0 or $\Delta F/F_0$. In analyses presented in Figures 2*d* and 3*c* peak F/F_0 or $\Delta F/F_0$ values were corrected for decaying fluorescence from the previous stimulus (Kochlamazashvili et al. 2010). The decay time constant of Ca^{2+}-dependent fluorescence did not differ between sham and heparinase-treated slices (monoexponential fit, sham 161.9 ± 13.0 ms, heparinase 137.1 ± 15.8 ms,

n = 29 and 17, unpaired t-test, P = 0.354). For recording of Ca^{2+} transients, the membrane potential was adjusted to −70 mV (either in voltage clamp or via a constant holding current). For Schaffer collateral stimulation (5× TBS; see above, Fig. 2), the stimulus intensity was set to 4× the intensity to induce a single action potential in a burst. The NMDAR inhibitor AP5 (50 µM) was added in these experiments to prevent Ca^{2+} indicator saturation and to reduce variability (a modulation of NMDAR-mediated synaptic transmission by heparinase treatment has been excluded, as shown in Fig. 1*b* and Supplementary Fig. 2*d*). Ca^{2+} responses to back-propagating action potentials (b-AP) were evoked by 2–3 ms long command jumps to +10 mV at a frequency of 20 Hz (Fig. 3). In a subset of experiments, saturation of the Ca^{2+} indicator Fluo-4 was induced using a high-frequency train of 80 bAPs at 100 Hz. Resting [Ca^{2+}] was estimated from the ratio F_0/F_{MAX} (see Supplementary Fig. 5*a*–*c*) (Ermolyuk et al. 2012). The low-affinity Ca^{2+} indicator OGB6F was used in a Cs^+-based intracellular solution (see above) to measure the nifedipine-sensitive component of sustained Ca^{2+} influx into dendrites and spines during 1 s of depolarization from −50 to +20 mV in presence of TTX, NBQX, AP5, PTX, and CGP52432 (see Supplementary Fig. 4). Line scans were repeated for up to 10 times for each region of interest.

2PE Fluorescence Lifetime Imaging

The fluorescence lifetime of OGB1 and its Ca^{2+}-dependent changes (Agronskaia et al. 2004; Zheng et al. 2015) were measured to obtain more quantitative information about the effect of HS removal on pyramidal cell Ca^{2+} signaling. Time-correlated single photon counting (TCSPC) was performed on a FV10MP Olympus microscope upgraded with a TCSPC module (Picoquant). OGB1 lifetimes were quantified using a photon count ratio (see Supplementary Fig. 3*a* for an illustration) and calibrated. Spatially and temporally resolved lifetime analysis was performed on frame scan and line scan data using custom written scripts (Matlab, Mathworks). OGB1 lifetime changes were monitored during 3 depolarizing voltage steps from −70 to +20 mV; step durations were either 25 or 400 ms, repeated at 1 Hz. Line scans were

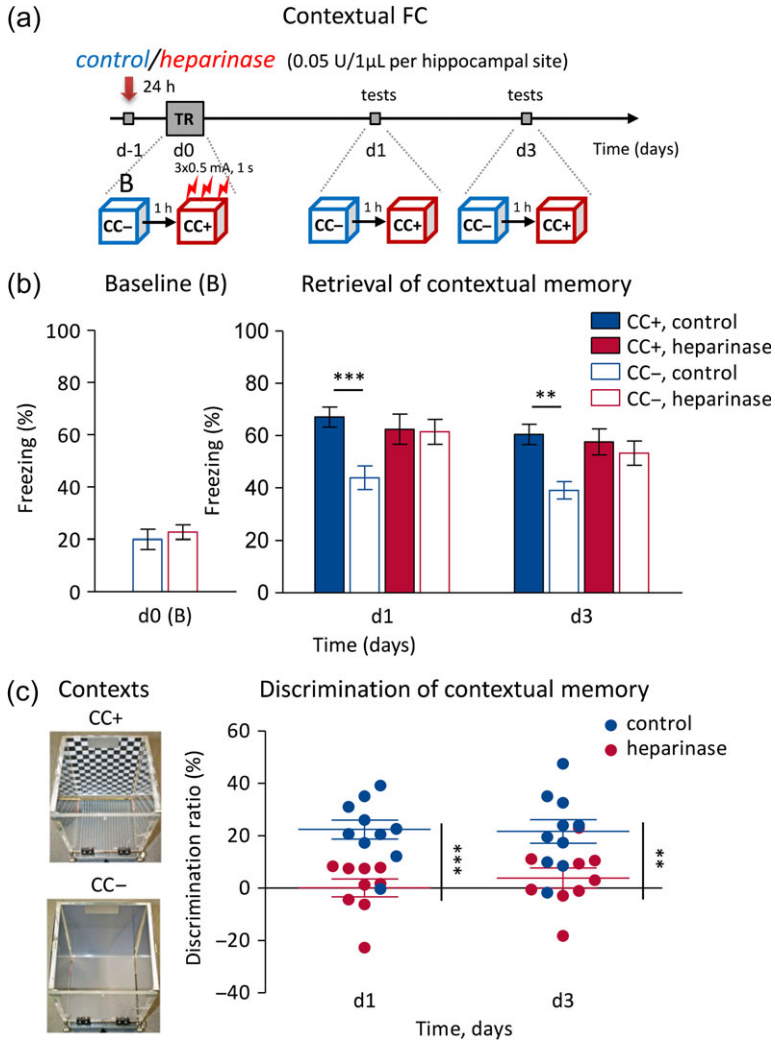

Figure 6. Intrahippocampal heparinase 1 injection impairs context discrimination in CFC. (*a*) Experimental design of CFC with injection of either active heparinase (heparinase) or heat-inactivated heparinase (control) 24 h before CFC. (*b*) The group of mice injected with heparinase showed normal level of freezing in a neutral context (CC–) before CFC on d0, and in the conditioned context (CC+) after CFC on d1 and d3. However, they were unable to discriminate the conditioned context (CC+, solid bars) from the unconditioned, neutral one (CC–, empty bars). (*c*) The discrimination ratio (%) of freezing in the 2 different contexts (at the left panel) after control/heparinase injection confirms the inability of mice to discriminate 2 different but similar contexts after HSs were removed by heparinase injection into the dorsal hippocampus.

repeated up to 6 times. To increase photon yield, TCSPC was performed during both scanning and retracing. Photon arrival times relative to the excitation pulse were accumulated over 20 ms bins, analyzed and subsequently converted into [Ca^{2+}] (Fig. 3*d*). Resting [Ca^{2+}] presented in Supplementary Figure 5*d* was taken as a mean of the baseline period.

Statistics

Numerical data are reported as mean ± SEM with *n* being the number of samples. In figures, asterisks indicate statistical significance (details in figure or figure legend). Student's *t*-tests and multiway ANOVA with suitable post-hoc tests were used as indicated and performed in Matlab (Mathworks), SPSS (IBM), and Origin (OriginLab) and *P* represents the level of significance. Significance levels are indicated in figures by asterisks (*$P < 0.05$, **$P < 0.01$, ***$P < 0.001$) unless stated otherwise.

Results

Removal of HSs Impairs LTP

HSPGs can interact with a plethora of cellular components and thereby modify synaptic transmission and plasticity. We first tested if enzymatic digestion of HSs affects synaptic transmission and its LTP. HSs were removed from acute slices by incubating slices in extracellular solution containing either heparinase 1 (1 U/mL) or heat-inactivated heparinase 1 (control treatment). This protocol was sufficient to cleave HSs in dissociated cultures and acute hippocampal slices (see Supplementary Fig. 1). We next tested if heparinase treatment affects excitatory synaptic transmission. This was investigated at CA3–CA1 Schaffer collateral synapses using field potential recordings (fEPSPs) (see Fig. 1*a*–*c*, Supplementary Fig. 2). To account for variable efficacy of axonal stimulation between slices and treatments, fEPSP slopes were normalized to the amplitude of the axonal fiber volley. No effect of heparinase treatment on fEPSPs could be detected over a range of stimulation intensities (see Fig. 1*b*, Supplementary Fig. 2*a*–*c*). Similarly, heparinase treatment did not affect NMDAR-mediated fEPSPs (see Fig. 1*b* and Supplementary Fig. 2*d*). A potential modulation of the presynaptic release probability by heparinase treatment was assessed by paired-pulse stimulation experiments. Again, no effect of heparinase treatment could be detected (see Fig. 1*c*, Supplementary Fig. 2*e*,*f*). Together, these observations indicate that heparinase treatment does not have a major impact on baseline excitatory transmission at this synaptic pathway. We next investigated LTP of synaptic transmission, because cleaving hyaluronic acid, another glycan, was previously shown to impair LTP at this synapse (Kochlamazashvili et al. 2010). LTP was induced by a single cycle or repeated TBS (Fig. 1*d*,*e*). We found no significant effect of heparinase treatment on LTP induced by a single cycle of TBS. However, when 5 cycles of TBS were delivered, an impairment of LTP in heparinase-treated slices was uncovered (Fig. 1*d*,*e*). LTP in slices receiving the control treatment (heat-inactivated heparinase) was not statistically different from native slices, which were not incubated (native 156.1 ± 5.9% vs. heat-inactivated heparinase 144.5 ± 4.8%, $n = 8$ both groups, $P = 0.15$, unpaired *t*-test). The reduction of LTP in heparinase-treated slices was not due to an effect on GABAergic synaptic inhibition, because the reduction persisted in the presence of the ionotropic GABA receptor inhibitor PTX (Fig. 1*e*). Together these results reveal a significant reduction of LTP induced by repeated TBS after removal of HSs without an effect on baseline excitatory transmission.

Impairment of Ca^{2+} Influx During LTP Induction

The dependence of LTP on postsynaptic intracellular Ca^{2+} signaling is well-established (Lynch et al. 1983). Therefore, we tested if a reduced Ca^{2+} entry during LTP induction underlies the LTP impairment observed after heparinase treatment. To this end, 2PE Ca^{2+} imaging was performed in spines and dendrites of CA1 pyramidal cells held in the whole-cell patch-clamp configuration (Ca^{2+} indicator Fluo-4, Materials and Methods) during TBS of CA3–CA1 Schaffer collateral synapses (Fig. 2). In order to decrease interexperiment variability, the intensity of axonal stimulation was set to 4× the current required for a single action potential to occur during a single test burst of 5 stimuli (control 71.6 ± 5.9 µA, heparinase 55.2 ± 6.2 µA, $n = 11$ both groups, $P = 0.19$, unpaired *t*-test, see also Kochlamazashvili et al. 2010) and NMDARs were inhibited by AP5 (NMDAR-dependent synaptic transmission was not affected by heparinase, see above and Materials and Methods). Indeed, the Ca^{2+}-dependent fluorescence transients evoked by TBS were reduced in heparinase-treated slices (Fig. 2*d*). This was not a consequence of indicator saturation, because a 2.5-fold higher stimulus intensity induced Fluo-4 fluorescence transients with 3–4-fold higher amplitudes ($P = 0.019$ and <0.001 for control and heparinase-treated slices, $n = 4$ and 6, unpaired *t*-tests). Thus, postsynaptic Ca^{2+} signals during TBS are reduced in heparinase-treated slices and this reduction is likely to underlie the observed reduction of LTP. Importantly, boosting Ca^{2+} entry during induction of LTP via L-type voltage-gated Ca^{2+} channels using BayK 8644 (15 µM) abolishes the effect of heparinase treatment on LTP (control + BayK 154.2 ± 6.6%, heparinase + BayK 151.6 ± 5.9, $n = 8$ both groups, unpaired *t*-test, $P = 0.77$). While this observation does not implicate L-type voltage-dependent Ca^{2+} channels (VGCCs) in the heparinase-induced reduction of Ca^{2+} entry during TBS, it demonstrates that the reduced Ca^{2+} entry is sufficient to explain the LTP deficit in heparinase-treated slices.

No Change of Depolarization-Induced Ca^{2+} Entry

To identify the mechanism underlying reduced Ca^{2+} entry during TBS, we further investigated how removal of HSs modifies Ca^{2+} signaling of CA1 pyramidal cells. VGCCs represent a main route of Ca^{2+} entry at spines and dendrites. We previously showed that hyaluronic acid, another component of the ECM, supports Ca^{2+} entry via L-type VGCCs and in turn LTP (Kochlamazashvili et al. 2010). Also, HSs can directly interact with L-type VGCC and thereby delay channel inactivation in HEK cells (Garau et al. 2015). Both observations suggest that removal of HSs from hippocampal slices could impair L-type channel function and thereby Ca^{2+} entry during TBS. This was tested by recording Ca^{2+} responses to trains of back-propagating action potentials (b-APs, 5 at 20 Hz, Fig. 3). However, no effect of heparinase treatment could be detected (Fig. 3*c*, $n = 16$ and 25 for control and heparinase treatment, 3-way repeated measures ANOVA, $P = 0.97$) irrespective of whether Ca^{2+} transients were recorded from spines or dendrites ($P = 0.79$).

Because dendritic APs could change their amplitude or width uncontrollably when propagating toward the recorded spines and dendrites, we also tested if Ca^{2+} responses evoked by somatic depolarization in voltage clamp are affected by heparinase treatment in the presence of the sodium channel blocker TTX and receptors antagonists (NBQX, AP5, PTX, CGP52432). To obtain a more quantitative estimate of Ca^{2+} concentrations and their changes, we used the Ca^{2+}-dependent fluorescence lifetime of OGB1 as a readout of Ca^{2+} concentrations (fluorescence lifetime imaging, FLIM [Agronskaia et al. 2004; Zheng et al.

2015], Supplementary Fig. 3). Somatic voltage steps from −70 to +20 mV for 25 ms triggered clearly detectable Ca^{2+} responses in spines and dendrites (see Fig. 3*d*, Supplementary Fig. 3c,*d*), which were not affected by dye saturation (see Supplementary Fig. 3c,*d*). Again, amplitudes of Ca^{2+} responses were not affected by heparinase treatment in spines or dendrites (Fig. 3*d*). However, a HS-dependent change of L-type VGCC inactivation may not be detectable during brief depolarizations. Therefore, a separate set of experiments using the low-affinity indicator Oregon Green 488 BAPTA 6F (OGB6F) with long depolarization was performed (see Supplementary Fig. 4). None of these experiments including pharmacological tests with the L-type VGCC inhibitor nifedipine suggested a modified behavior of VGCCs after heparinase treatment. Finally, the resting Ca^{2+} concentration of dendrites and spines was not different between heparinase and sham treated slices (see Supplementary Fig. 5). Thus, the impaired Ca^{2+} entry during TBS observed in slices after heparinase incubation is not caused by a reduced availability or activity of VGCC channels.

Heparinase Treatment Reduces Pyramidal Cell Excitability

The absence of an effect of heparinase treatment on Ca^{2+} entry induced by somatic voltage step commands and b-APs prompted us to explore if the decreased Ca^{2+} influx during TBS could be a consequence of reduced action potential firing of pyramidal cells. To address this, the number of action potentials fired by pyramidal cells during TBS was analyzed for each burst during TBS (Fig. 4*a*,*b*). This analysis revealed a significant reduction of spikes generated per burst when HSs had been removed by heparinase treatment (Fig. 4*b*). Such a decrease of spikes fired per burst can have its origin upstream of the soma and axon, for example a dampened dendritic integration of synaptic input, or at the site of action potential generation itself, for example reduced excitability of the AIS. To differentiate between the 2 scenarios, 40 ms long current pulses mimicking the TBS pattern were injected into CA1 pyramidal cells (Fig. 4*c*). Similar to synaptic TBS, the current pulse amplitude was set in each individual neuron to 4× the current required for a single spike upon a single current injection (no difference of currents between treatments, Supplementary Fig. 7*d*). Analysis of the average spike number per burst revealed a significant reduction of spiking in heparinase-treated slices, which was similar to that observed during synaptic TBS (Fig. 4*c*,*d*). This heparinase-induced reduction of pyramidal cell excitability is sufficient to explain the lower number of spikes generated during synaptic TBS in heparinase-treated slices, and also the reduced Ca^{2+} entry and LTP. Having already excluded an effect of heparinase treatment on synaptic transmission, this result also strongly suggests that removal of HSs is affecting spike generation in the AIS. One indicator of axonal excitability is the spike threshold (Scott et al. 2014), which was therefore analyzed. Indeed, we found that the second but not the first spike threshold was increased by heparinase treatment (Fig. 4*e*). This increase of the spike threshold became prominent during later bursts, matching the progressive reduction of spike numbers per burst (Fig. 4*d*). An axonal site of action of heparinase is also indirectly suggested by the absence of a heparinase effect on various other cell parameters. The peak spike voltage and maximum rate of depolarization represent indicators of somatic sodium channel availability. Neither was affected by heparinase treatment (see Supplementary Fig. 6). Also, no effect on the somatic membrane potential, the input resistance, the IH-dependent sag potential, the spike width or the medium after hyperpolarization was found (see Supplementary Figure Legend 6 and Supplementary Fig. 7).

To gain further insight into the mechanism of heparinase action, action potential trains were evoked by longer-lasting current injections of increasing amplitude (Fig. 4*f*, left panel). Again, a spike threshold increase was observed in heparinase-treated slices (Fig. 4*f*, right panel). However, the effect on the spike threshold became prominent only when stronger stimuli were used. This is in line with 2 previous observations in our present study. First, the current threshold for triggering a single spike within 40 ms (or 300 ms) of stimulus onset is not affected by removal of HSs (see Supplementary Fig. 7*d*). Second, stronger stimuli with a TBS pattern do reveal the reduced excitability (see above, Fig. 4*a*–*d*). Thus, the experimental evidence suggests a role of HSs for maintaining spiking in response to strong input at the AIS.

We, therefore, tested if heparinase treatment modifies the AIS. The protein AnkG is the master organizer of the AIS (Yoshimura and Rasband 2014). Its axonal distribution indicates the position and length of the AIS and changes of AnkG labeling accompany structural changes of the AIS, which affect properties of action potential firing such as the current threshold and repetitive firing (Grubb and Burrone 2010; Yoshimura and Rasband 2014). Immunohistochemistry using an antibody against AnkG was performed on dissociated hippocampal cultures that received either a control or heparinase treatment (see Supplementary Fig. 8). We found that heparinase treatment selectively reduced the distal but not proximal AnkG label, which indicates that the integrity of distal AIS is reduced while the distance from the soma to the AIS start is not affected after digestions of HSs. To confirm these results in acute slices, we used heparinase-treated and control slices obtained from Thy1-YFP transgenic mice, in which a subset of CA1 pyramidal cells express the fluorescent protein YFP (Fig. 5*a*). The distance from the AIS start to the soma-hillock transition was analyzed first (blinded to experimental condition). The start of the AIS was visually identified as the region where AnkG labeling displayed a sharp rise. Its distance to the soma-hillock transition was not affected by heparinase treatment (control 4.6 ± 0.26 µm, n = 135; heparinase 4.7 ± 0.23 µm, n = 154; P = 0.74, unpaired t-test), which is in agreement with our observations in dissociated cultures. However, we noted a considerable variability of the AIS start (see Supplementary Fig. 9, coefficient of variation >0.6 both groups) and also of the trajectories of axons in all 3 dimensions. Therefore, we selected only axons for further analysis that stayed within 5 µm of the focal plane containing the axonal hillock (along the z-axis, to avoid errors introduced by depth-dependent changes of fluorophore excitation and emission) and that had their AIS start within mean ± 3 × SEM. Seventeen axons from control and 21 from heparinase-treated slices fulfilled these criteria and their axonal AnkG profiles were averaged (Fig. 5*b*,*c*). As predicted by experiments in dissociated cultures, the distal but not proximal axonal AnkG label was significantly reduced by heparinase treatment (Fig. 5*d*,*e*). This indicates that, indeed, HSs have a role in maintaining the AIS.

In previous work (Scott et al. 2014), we have demonstrated that repetitive firing expands the initially proximal and narrow action potential initiation site further into the axon of DG granular cells. A reduced integrity of the distal AIS after heparinase treatment is, therefore, expected to selectively affect later spikes during repetitive firing, which is in good agreement with the experimentally observed spiking behavior after heparinase treatment (Fig. 4).

Impairment of CFC

We next asked what the behavioral relevance of the LTP deficit after heparinase treatment might be. Selective impairment of LTP induced by strong stimuli at CA3–CA1 synapses has previously been associated with a deficit in CFC (Kochlamazashvili et al. 2010) or context discrimination (Jin et al. 2013). Therefore, we tested if heparinase treatment impairs fear conditioning or context discrimination in a CFC paradigm (Fig. 6*a*, see Materials and Methods). Injection of heparinase did not affect the level of spontaneous freezing/immobility before CFC at d0 in the neutral context (CC–) compared with control treatment (both conditions ~20% freezing, Fig. 6*b*). This level of freezing before CFC is expected because mouse movement could be slightly constrained by the cable connection to the recording system (typical freezing level during fully unconstrained exploration of novel environment is 5–10% in mice).

Of note, 48 and 96 h after intrahippocampal heparinase injection, that is at d1 and d3, respectively, control- and heparinase-injected mice showed similar freezing in the conditioned context (CC+, Fig. 6*b*). Freezing times were 62.4 ± 5.7% (d1) and 57.6 ± 5.0% (d3) in heparinase-injected mice (n = 9) and 67.1 ± 3.8% (d1) and 60.5 ± 3.9% (d3) after control treatment (n = 10, repeated measures 2-way ANOVA: treatments P = 0.507, days P = 0.103). However, the freezing time in neutral contexts (CC–) was significantly different (P = 0.0093) between treatment groups and the test day was a significant factor (P = 0.031). Heparinase-injected mice froze in CC– as long as in CC+ (61.4 ± 4.7% and 53.3 ± 4.6% at d1 and d3, respectively) whereas the control group froze in CC– less than in CC+ (43.9 ± 4.5% and 39.1 ± 3.3% at d1 and d3, respectively; CC+ vs. CC– in the control group P < 0.001 at both days; CC+ vs. CC– in heparinase-injected animals P > 0.3 at both days; paired t-tests). We, therefore, calculated the context discrimination ratio ([Freezing% in CC+] – [Freezing% in CC–])/ ([Freezing% in CC+] + [Freezing% in CC–]), which revealed the inability of heparinase-injected mice to discriminate between the conditioned context CC+ and the unconditioned neutral CC– at any testing days (Fig. 6*c*), unlike control mice (P < 0.005 at d1 and P < 0.01 at d3).

Reduction of Oscillatory Network Activity In Vivo by Heparinase Treatment

In vivo, hippocampal neuronal activity can be synchronized in different frequency bands depending on the behavioral state. These hippocampal oscillations, in particular those at the theta frequency range, are implicated in many learning and memory processes in humans and animals (Colgin 2016). Therefore, we explored how low theta (Lθ, 4–7 Hz) and high theta (Hθ, 7–10 Hz) oscillations during CFC are affected by context, behavior and heparinase treatment (Fig. 7). Frequency analysis in the θ range revealed that when mice were actively exploring their environment, theta activity peaked in Hθ. However, when mice were freezing, independent of context, theta peak activity was shifted to Lθ (Fig. 7*a*–*d*). This shift was highly significant in both treatment groups (P < 0.0005) and was stable over time. The θ peak frequency during freezing (fr) events stayed within Lθ range around 6 Hz (5.8 ± 0.4 – 7 ± 0.4 Hz) for both treatment groups and recording areas (CA1 *stratum pyramidale* and DG *stratum moleculare*, Fig. 7*e*). Similarly, the θ peak frequency during exploration (exp) was mostly in the Hθ band ranging from 7.9 ± 0.2 to 9.1 ± 0.2 Hz (Fig. 7*e*).

Statistical analysis (general linear model with repeated measures; 4 within-subject factors: context, behavior, day after CFC, brain region; one between-subject factor: heparinase/control treatment) showed that only one factor, behavior (freezing versus exploration), highly significantly (P < 0.0005) modulated the θ frequency at d1 and d3. Furthermore, there were significant interactions between treatment and context (P = 0.003), as well as between treatment and day (P = 0.009). At d0, only data recorded in the CC– context were available for analysis of the θ frequency shift by design (Fig. 7*e*, left panel). To compare θ frequency shifts over the entire duration of the CFC experiments, another analysis was performed using only data obtained in CC– but from d0, d1, and d3. Again, analysis showed that only behavior (P < 0.0005) modulated the θ frequency. In addition, we found interactions between treatment and day (P = 0.023) as well as between day and behavior (P = 0.006) probably reflecting the fact that at d0 the peak Hθ (~9 Hz) was slightly higher compared with d1 and d3 (~8 Hz). To conclude, neither heparinase treatment nor context alone influenced the main θ frequency during exploratory and freezing behavior in mice.

We next tested if the degree of network synchronization is affected by heparinase treatment. Spectral power is a useful measure of synchronization of neuronal activity near the recording electrode. To compare the power of Lθ oscillations (4–7 Hz) during freezing versus exploration events, we normalized Lθ power during freezing over Lθ power during exploration in both contexts (CC+/CC–). We found that Lθ power doubled during freezing in CC+ at d1/d3, without an effect of heparinase treatment (Fig. 7*f*). However, statistical analysis based on the general linear model with repeated measures indicated a significant interaction between context and treatment at d1 and d3 (P = 0.003). This reflects that in control mice the relative Lθ power in CC+ during freezing tended to be higher than in CC–, whereas in the heparinase-treated group the relative Lθ power in CC– during freezing tended to be higher compared with CC+. This correlates well with a higher freezing of heparinase-injected mice in CC– and the loss of contextual discrimination after heparinase injection. Also, the relative Lθ power was different between treatment groups at d1 in CC– (DG only, repeated measures 2-way ANOVA, P < 0.05).

Finally, we investigated Lθ power changes during CFC in heparinase-injected animals and control animals (Fig. 7*g*,*h*). There was no difference between treatment groups in Lθ during baseline recordings. However, the control group showed a 2-fold increase of Lθ power at post-training days d1 and d3 in both CC+ and CC– contexts (Fig. 7*g*) compared with the baseline preconditioning level at d0. In contrast, the network activity in the Lθ band of heparinase-injected animals was not elevated after CFC. Instead, the power of Lθ oscillations after CFC was almost unaffected at d1 and slightly elevated at d3 compared with the baseline period before CFC (Fig. 7*g*,*h*). Analysis revealed no strongly significant effect of context (P = 0.07) or brain region (P = 0.071). However, several other parameters significantly contributed to the Lθ changes: day (P = 0.01), brain region and day (P = 0.023) as well as heparinase treatment (P = 0.016).

Thus, the heparinase-induced impairment of context discrimination in CFC is associated with 2 distinct effects on theta oscillations. Heparinase injection affected the Lθ power increase during freezing after CFC in a context-dependent manner and prevented the post-CFC increase of Lθ power.

Discussion

The acute contribution of HSs to hippocampal function was identified in vitro and in vivo by enzymatic digestion of HSs. We found a distinct deficit of LTP of CA3–CA1 Schaffer

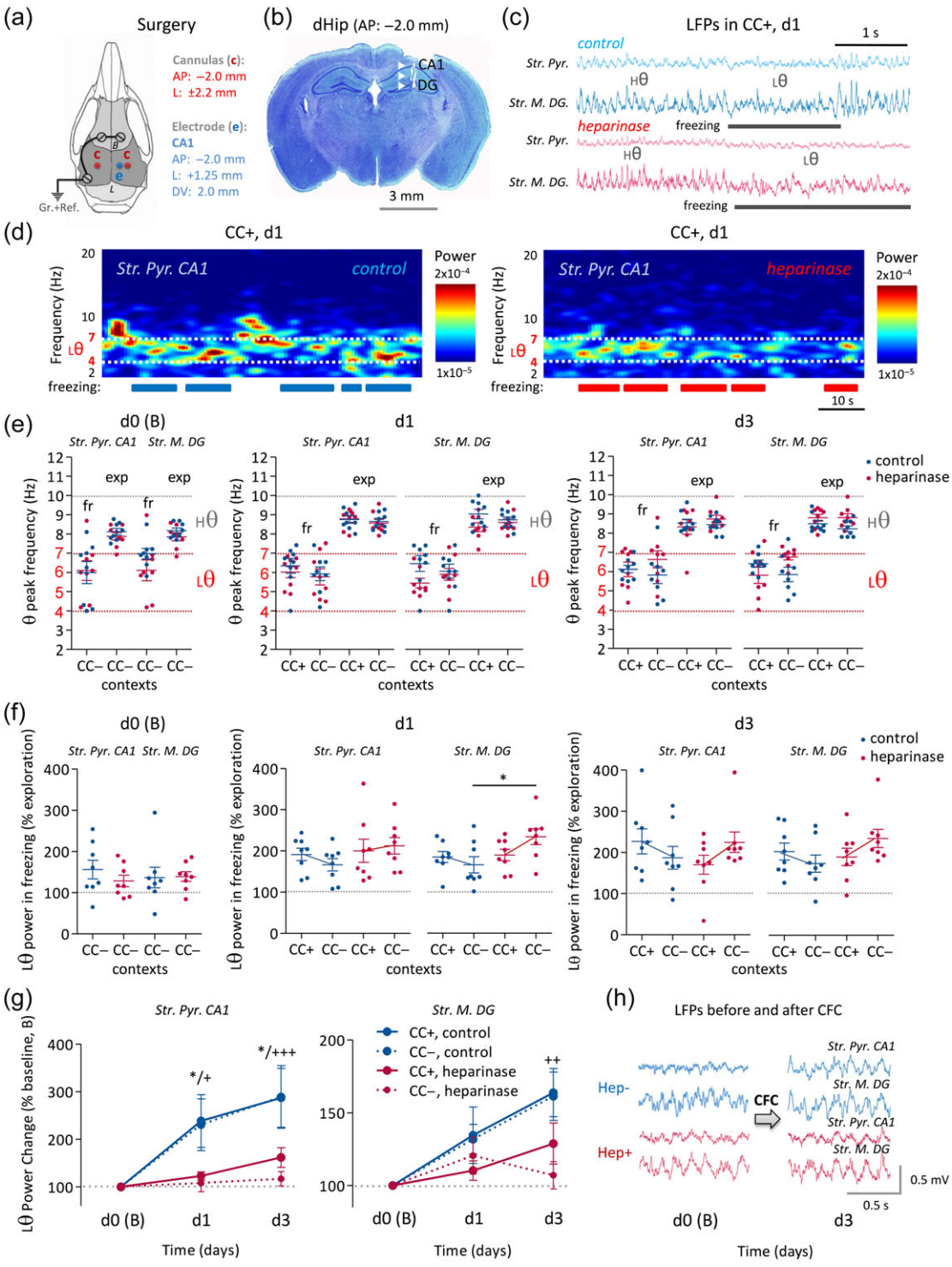

Figure 7. Theta oscillations during CFC are modified by intrahippocampal heparinase injection. (*a*) Schematic of surgical implantation of hippocampal electrodes and cannulas into a mouse brain with given coordinates and specific arrangement for a HIME system (Senkov et al. 2015). (*b*) Nissl staining of a brain section with located electrode tracks at the right dorsal hippocampus depicting the tips of the deepest electrodes at the DG and the most superficial electrodes at pyramidal cell layer of CA1. (*c*) Representative epochs of LFPs in both recorded areas (CA1 and DG) and in both treatment groups showing high theta oscillations (HΘ: 7–10 Hz) while mice explore the conditioned context (CC+) and low theta (LΘ: 4–7 Hz) when they freeze. (*d*) Representative examples of spectrograms of low frequency oscillations (2–20 Hz) in CC+ for 5 min at d1 after heparinase or control injection. Low theta oscillations show high power specifically at freezing events, while high theta appears only during exploration/motion epochs. Heparinase-injected mice show a reduction in power of low theta oscillations during retrieval of CFC memory traces versus control. (*e*) Analysis of θ peak frequency over all recording days shows a θ frequency shift from HΘ (7–10 Hz) to LΘ (4–7 Hz) of both treatment groups when mice explore (exp) either context (CC+/CC−) and freeze (fr). (*f*) Analysis of relative LΘ power during freezing normalized over LΘ power during exploration behavior shows a distinct increase (~100%) of LΘ power during freezing in CC+ and a lower increase in CC− in control mice. In heparinase-injected animals, a qualitatively opposite effect was detected, that is LΘ power increased in CC− during freezing more than in CC+. (*g*, *h*) The averaged low (4–7 Hz) theta power after CFC was normalized to the prefear conditioning level (baseline, B). A prominent increase of LΘ power can be detected after CFC in control experiments but not in heparinase-injected animals (sample traces in *h*; * significant difference of theta power in CC+ contexts between 2 treatment groups; +, ++, +++ significant difference of theta power in CC− contexts between 2 treatment groups).

collateral synapses after removal of HSs when a strong LTP-inducing paradigm was used in vitro. A reduced Ca^{2+} entry during LTP induction was identified as the underlying mechanism. This was not caused by alterations of excitatory or inhibitory synaptic transmission, but by a reduced axonal excitability of CA1 pyramidal cells. In vivo, removal of HSs was accompanied by a loss of context discrimination and abnormalities in Lθ oscillations.

HSs Regulate LTP and CA1 Pyramidal Cell Excitability

Previous studies have implicated HSPGs as contributors to synaptic plasticity. For instance, genetic deletion of the HSPG syndecan-3 improved LTP of CA3–CA1 synapses (Kaksonen et al. 2002). In contrast, enzymatic removal of HSs using heparinase 3 decreased LTP at the same pathway (Lauri et al. 1999), but the cellular mechanism has remained unclear.

We now demonstrate that specific removal of highly sulfated HSs with heparinase 1 results in impaired LTP that is only detected when strong LTP-inducing stimuli are used. This was not the consequence of altered baseline excitatory synaptic transmission at CA3–CA1 synapses, in line with a previous study (Lauri et al. 1999). Instead, we observed a reduction of Ca^{2+} influx during LTP induction in HSs deficient hippocampal slices. This reduced Ca^{2+} influx is sufficient to explain the LTP deficit, because pharmacological boosting of Ca^{2+}-entry using the L-type VGCC modulator BayK 8644 was sufficient to restore LTP. At the surface, these functional consequences of HSs removal are similar to observations after digestion of hyaluronic acid (Kochlamazashvili et al. 2010). In both cases, a reduced Ca^{2+} influx during LTP induction and decreased LTP was observed. However, mechanistically both ECM components control LTP differently. Hyaluronic acid is required for maintenance of somatodendritic L-type VGCC function in hippocampal neurons. In contrast, HSs do not appear to affect L-type VGCCs at these cells but rather support axonal excitability. Several experimental findings are in line with this conclusion.

First, no modulation of Ca^{2+} entry in response to b-APs or direct depolarization was detected using electrophysiology in combination with intensity and lifetime-based Ca^{2+} imaging. Therefore, an altered function of somatodendritic VGCCs at CA1 pyramidal cells cannot explain the decreased Ca^{2+} entry after heparinase treatment. This appears to be at odds with experiments in HEK293 cell transfected with L-type VGCC, in which HSs modulated voltage-dependent inactivation of Ba^{2+} currents (Garau et al. 2015). However, these culture experiments were done in the absence of Ca^{2+}, which was not the case in present experiments even though they were performed in the presence of high-affinity Ca^{2+} indicators. Therefore, Ca^{2+}-dependent inactivation in the present experiments may mask the voltage-dependent effects of heparinase treatment on VGCC function found in cultures. Thus, in physiological settings, that is with fully intact intracellular Ca^{2+} signaling, a direct modulation of VGCCs by HSs is likely to play a minor role. Second, the number of action potentials fired by CA1 pyramidal cells during LTP induction was significantly reduced in heparinase-treated slices and this effect could be reproduced by strong somatic current injections. Because the action potential-induced Ca^{2+} entry is not different between control and heparinase-treated slices, the reduced number of action potentials during LTP induction in heparinase-treated slices explains the decrease of Ca^{2+} entry during LTP induction. A plausible cause of reduced spiking is the increased threshold of action potentials in heparinase-treated slices. This increase of the spike threshold did only become apparent during TBS-like and strong current injections (Fig. 4*e*,*f*, see also Supplementary Figure Legend 7). Also, it was not accompanied by changes of the somatic spike waveform, which would have suggested an involvement of somatic sodium channel inactivation or other mechanisms that would alter somatic sodium channel density/availability. In addition, none of the parameters of CA1 pyramidal cell excitability that were monitored at the soma were affected by heparinase treatment. Thus, a selective modulation of axonal excitability or action potential initiation by HSs represents the most parsimonious explanation of our electrophysiological observations.

The AIS is the site of action potential generation. Its geometry, location, and the distribution and availability of its ion channels dynamically determine the site and threshold of spike initiation (Kole and Stuart 2012; Yoshimura and Rasband 2014). AnkG is a key organizing molecule of the AIS and important for ion channel clustering at the AIS and thus sets key parameters of neuronal spiking (Grubb and Burrone 2010; Kole and Stuart 2012; Yoshimura and Rasband 2014). In our experiments, heparinase treatment selectively reduced the distal but not proximal axonal density of AnkG. Given the importance of AnkG in orchestrating the clustering of ion channels in the AIS, the reduced presence of AnkG is expected to profoundly impair ion channel clustering in the distal AIS after heparinase treatment. Interestingly, we have previously observed in DG granular cell axons that the action potential initiation site is initially proximal and narrow but widens and extends further into the axon during repetitive spiking (Scott et al. 2014). This indicates that the impairment of the distal AIS may only manifest during repetitive spiking, which is in good agreement with our experimental observations. Thus, HSs help maintain distal AIS integrity and as a consequence repetitive spiking. This could involve changes of, for instance, sodium or potassium channel density in the distal AIS.

Interestingly, the HSPG perlecan is recruited by dystroglycan to nodes of Ranvier, where it binds gliomedin and enhances clustering of node of Ranvier components (Colombelli et al. 2015). Although perlecan may play a more prominent role in organizing the AIS in the peripheral nervous system (Colombelli et al. 2015), all major HSPGs including perlecan are expressed in the hippocampus (Karthikeyan et al. 1994; Shee et al. 1998; Lauri et al. 1999). Moreover, NrCam and Neurofascin-186 are 2 molecules that establish a link between the ECM and AnkG and are thus thought to contribute to sodium and potassium channels clustering (Nav1.x, Kv1, and Kv7 families) (Dityatev et al. 2010; Rasband 2010). In addition, other components of the ECM like tenascins may also affect sodium channel clustering/activity in the AIS (Srinivasan et al. 1998). To summarize, the most likely scenario is that heparinase treatment disrupts the AIS ECM and modifies distal AnkG levels and ion channel clustering. A number of interesting questions for future work emerge from our findings. For instance, it remains to be shown that removal of HSs specifically at the AIS is responsible for the observed effects. It will also be interesting to dissect if the observed reduction of AIS excitability is primarily caused by a reduction of distal AIS potassium or sodium channels clustering or both. In addition, it remains to be established, if the impairment of LTP and neuronal excitability after HS removal are specific to the CA1 region or a ubiquitous effect.

Previous studies revealed the importance of interaction between HSPG syndecan-3—heparin-binding growth-associated protein (HB-GAM or pleiotrophin) in synaptic plasticity (Lauri et al. 1999; Kaksonen et al. 2002; Pavlov et al. 2002). However, mice deficient in syndecan-3 exhibited enhanced rather than reduced LTP (Kaksonen et al. 2002), and hence do not mimic the

effect of heparinase 1. Moreover, syndecan-3 seems to act via postsynaptic mechanisms rather than by influencing axonal excitability (Lauri et al. 1999; Melendez-Vasquez et al. 2005). Thus, our experiments revealed a novel function of HSs in neuronal excitability and LTP that is mediated by proteoglycans carrying highly sulfated HSs. The specific effects observed after heparinase 1 treatment may be related to a loss of specific glycoepitopes or to the generation of novel molecular recognitions sites with a terminal glucosamine, which are distinct from *N*-acetylglucosamine-containing sites generated by heparinase 3.

HSs Support Learning and Learning-Related Network Oscillations

Our data provide the first evidence that a specific and acute modification of HSs in the adult brain, that is cleavage of highly sulfated HSs in the hippocampus, can lead to impairment of context discrimination, but not learning per se. A similar combination of an impairment of context discrimination and modified LTP in the CA1 region in vitro has also been observed in other studies. For instance, inhibition of the Ras-GRF1 pathway in the CA1 region modulated LTP and context discrimination (Jin et al. 2013; Darcy et al. 2014). Thus, the present study uncovers a contribution of HSs for hippocampal LTP and context discrimination and also supports the notion that the CA1 region is involved in context discrimination (Place et al. 2012; Czerniawski and Guzowski 2014).

We also uncovered several interesting relationships between hippocampal θ oscillations, behavior, and removal of highly sulfated HSs by heparinase. First, the transition from exploration to freezing was accompanied by a shift from high to low θ oscillations independently of treatment. A similar Hθ to Lθ shift was first described by Seidenbecher et al. (2003), who provided examples illustrating that theta activity between 7 and 10 Hz prevails in the CA1 during risk-assessment behavior, and θ activity between 4 and 5 Hz appears in the lateral amygdala and CA1 during freezing. Qualitatively similar observations have been documented in various other studies (Machado et al. 2012; Ognjanovski et al. 2014; Tendler and Wagner 2015). Thus, a high to low theta frequency shift is strongly associated with freezing behavior. However, this relationship was not profoundly affected by removal of highly sulfated HSs and does, therefore, not explain the impaired context discrimination after heparinase injection.

In contrast, we found that fear conditioning increased the power of Lθ oscillations in control but much less in heparinase-injected animals. This effect was particularly prominent in the CA1 region and correlated well with the impaired excitability and LTP in the same region in vitro. It is intuitive that a reduced excitability of pyramidal cells reduces the power of network oscillations. For instance, recordings from mice with reduced activity of Nav1.6, a sodium channel enriched at the AIS, and nodes of Ranvier display a reduction of the θ power in awake animals (Pal et al. 2015).

This absence of a Lθ oscillations power increase after CFC in heparinase-injected animals was associated with impaired context discrimination. The most parsimonious explanation for these findings is that an Lθ oscillations power increase is required for successful context discrimination in CFC. Indeed, available data suggest that CA1 Lθ power is a predictor for successful fear-driven memory retrieval in rodents. For instance, the muscarinic cholinergic antagonist scopolamine disrupts CFC (Anagnostaras et al. 1999) whereas M1/M4 agonists improve CFC in aged mice (Si et al. 2010). At the same time, cholinergic innervation powerfully modulates hippocampal theta oscillation power and coherence (Hasselmo 2006; Vandecasteele et al. 2014). Also, inactivation of the ventral tegmental area with procaine in rats leads to impaired fear conditioning and decreased θ power of CA1 specifically at the Lθ frequency range (3–6 Hz) during immobility states, whereas control rats exhibit an increases in θ power after fear conditioning (Matulewicz et al. 2015). Therefore, we speculate that interfering with increase of Lθ may impair learning and/or retrieval of context memories or, as our data suggest, introduce an error in discrimination of 2 similar but yet different contexts.

Conclusion

In this study, we have explored the contribution of highly sulfated HSs to hippocampal function and behavior. Their acute removal impairs synaptic LTP by lowering postsynaptic axonal excitability in vitro. In vivo, we demonstrate a role of HSs in modulating theta oscillation and context discrimination in a fear conditioning paradigm. It remains to be established to what degree pyramidal cell excitability alone explains our in vivo observation and if changes of, for instance, interneuron function are involved too. Nonetheless, our results demonstrate that HSs are continuously required in the adult brain to maintain hippocampal plasticity and hippocampus-dependent memory.

Supplementary Material

Supplementary material are available at *Cerebral Cortex* online.

Funding

The NRW-Rückkehrerprogramm (C.H.), Human Frontiers Science Program (C.H., HFSP RGY-0084/2012), UCL Excellence Fellowship (C.H.), BMBF (A.D., 01EW1308A) and EraNet TargetECM (A.D.), and German Research Foundation (DFG, C.H., SFB1089 B03, SPP1757 HE6949/1 and HE6949/3).

Notes

We thank Dr Zheng and Dr Rusakov (University College London, UK) for help with setting up fluorescence lifetime imaging. *Conflict of Interest*: None declared.

References

Agronskaia AV, Tertoolen L, Gerritsen HC. 2004. Fast fluorescence lifetime imaging of calcium in living cells. J Biomed Opt. 9:1230–1237.

Anagnostaras SG, Maren S, Sage JR, Goodrich S, Fanselow MS. 1999. Scopolamine and Pavlovian fear conditioning in rats: dose-effect analysis. Neuropsychopharmacology. 21:731–744.

Anders S, Minge D, Griemsmann S, Herde MK, Steinhäuser C, Henneberger C. 2014. Spatial properties of astrocyte gap junction coupling in the rat hippocampus. Phil Trans R Soc B. 369: 20130600.

Colgin LL. 2016. Rhythms of the hippocampal network. Nat Rev Neurosci. 17:239–249.

Colombelli C, Palmisano M, Eshed-Eisenbach Y, Zambroni D, Pavoni E, Ferri C, Saccucci S, Nicole S, Soininen R, McKee KK, et al. 2015. Perlecan is recruited by dystroglycan to nodes of Ranvier and binds the clustering molecule gliomedin. J Cell Biol. 208:313–329.

Czerniawski J, Guzowski JF. 2014. Acute neuroinflammation impairs context discrimination memory and disrupts pattern separation processes in hippocampus. J Neurosci. 34: 12470–12480.

Dam GB, ten, Hafmans T, Veerkamp JH, Kuppevelt TH van. 2003. Differential expression of heparan sulfate domains in rat spleen. J Histochem Cytochem. 51:727–739.

Darcy MJ, Jin S-X, Feig LA. 2014. R-Ras contributes to LTP and contextual discrimination. Neuroscience. 277:334–342.

Dityatev A, Dityateva G, Sytnyk V, Delling M, Toni N, Nikonenko I, Muller D, Schachner M. 2004. Polysialylated neural cell adhesion molecule promotes remodeling and formation of hippocampal synapses. J Neurosci. 24:9372–9382.

Dityatev A, Seidenbecher CI, Schachner M. 2010. Compartmentalization from the outside: the extracellular matrix and functional microdomains in the brain. Trends Neurosci. 33:503–512.

Ermolyuk YS, Alder FG, Henneberger C, Rusakov DA, Kullmann DM, Volynski KE. 2012. Independent regulation of basal neurotransmitter release efficacy by variable ca(2+) influx and bouton size at small central synapses. PLoS Biol. 10: e1001396.

Feng G, Mellor RH, Bernstein M, Keller-Peck C, Nguyen QT, Wallace M, Nerbonne JM, Lichtman JW, Sanes JR. 2000. Imaging neuronal subsets in transgenic mice expressing multiple spectral variants of GFP. Neuron. 28:41–51.

Garau G, Magotti P, Heine M, Korotchenko S, Lievens PM-J, Berezin V, Dityatev A. 2015. Heparin/heparan sulfates bind to and modulate neuronal L-type (Cav1.2) voltage-dependent Ca2+ channels. Exp Neurol. 274 (Part B):156–165., Deciphering sugar chain-based signals regulating integrative neuronal functions.

Grubb MS, Burrone J. 2010. Activity-dependent relocation of the axon initial segment fine-tunes neuronal excitability. Nature. 465:1070–1074.

Hasselmo ME. 2006. The role of acetylcholine in learning and memory. Curr Opin Neurobiol. 16:710–715.

Heeroma JH, Henneberger C, Rajakulendran S, Hanna MG, Schorge S, Kullmann DM. 2009. Episodic ataxia type 1 mutations differentially affect neuronal excitability and transmitter release. Dis Model Mech. 2:612–619.

Henneberger C, Rusakov DA. 2012. Monitoring local synaptic activity with astrocytic patch pipettes. Nat Protoc. 7: 2171–2179.

Irie F, Badie-Mahdavi H, Yamaguchi Y. 2012. Autism-like sociocommunicative deficits and stereotypies in mice lacking heparan sulfate. Proc Natl Acad Sci USA. 109:5052–5056.

Jin S-X, Arai J, Tian X, Kumar-Singh R, Feig LA. 2013. Acquisition of contextual discrimination involves the appearance of a RAS-GRF1/p38 mitogen-activated protein (MAP) kinase-mediated signaling pathway that promotes long term potentiation (LTP). J Biol Chem. 288:21703–21713.

Kaksonen M, Pavlov I, Võikar V, Lauri SE, Hienola A, Riekki R, Lakso M, Taira T, Rauvala H. 2002. Syndecan-3-deficient mice exhibit enhanced LTP and impaired hippocampus-dependent memory. Mol Cell Neurosci. 21:158–172.

Karthikeyan L, Flad M, Engel M, Meyer-Puttlitz B, Margolis RU, Margolis RK. 1994. Immunocytochemical and in situ hybridization studies of the heparan sulfate proteoglycan, glypican, in nervous tissue. J Cell Sci. 107:3213–3222.

Kochlamazashvili G, Henneberger C, Bukalo O, Dvoretskova E, Senkov O, Lievens PM-J, Westenbroek R, Engel AK, Catterall WA, Rusakov DA, et al. 2010. The extracellular matrix molecule hyaluronic acid regulates hippocampal synaptic plasticity by modulating postsynaptic L-type Ca2+ channels. Neuron. 67:116–128.

Kole MHP, Stuart GJ. 2012. Signal processing in the axon initial segment. Neuron. 73:235–247.

Korotchenko S, Cingolani LA, Kuznetsova T, Bologna LL, Chiappalone M, Dityatev A. 2014. Modulation of network activity and induction of homeostatic synaptic plasticity by enzymatic removal of heparan sulfates. Phil Trans R Soc B. 369:20140134.

Lauri SE, Kaukinen S, Kinnunen T, Ylinen A, Imai S, Kaila K, Taira T, Rauvala H. 1999. Regulatory role and molecular interactions of a cell-surface heparan sulfate proteoglycan (N-syndecan) in hippocampal long-term potentiation. J Neurosci. 19: 1226–1235.

Lynch G, Larson J, Kelso S, Barrionuevo G, Schottler F. 1983. Intracellular injections of EGTA block induction of hippocampal long-term potentiation. Nature. 305:719–721.

Machado BS, Kunicki ACB, Morya E, Sameshima K. 2012. Spectral characteristics of the hippocampal LFP during contextual fear conditioning. Einstein (Sao Paulo). 10:140–144.

Matsuo I, Kimura-Yoshida C. 2014. Extracellular distribution of diffusible growth factors controlled by heparan sulfate proteoglycans during mammalian embryogenesis. Phil Trans R Soc B. 369:20130545.

Matulewicz P, Orzeł-Gryglewska J, Braszka Ł, Zawistowski P, Jurkowlaniec E. 2015. Hippocampal theta rhythm after local administration of procaine or amphetamine into the ventral tegmental area in fear conditioned rats. Neurosci Lett. 589: 132–137.

Melendez-Vasquez C, Carey DJ, Zanazzi G, Reizes O, Maurel P, Salzer JL. 2005. Differential expression of proteoglycans at central and peripheral nodes of Ranvier. Glia. 52:301–308.

Ognjanovski N, Maruyama D, Lashner N, Zochowski M, Aton SJ. 2014. CA1 hippocampal network activity changes during sleep-dependent memory consolidation. Front Syst Neurosci. 8:61.

Pal D, Jones JM, Wisidagamage S, Meisler MH, Mashour GA. 2015. Reduced Na v 1.6 sodium channel activity in mice increases in vivo sensitivity to volatile anesthetics. PLoS One. 10:e0134960.

Pavlov I, Võikar V, Kaksonen M, Lauri SE, Hienola A, Taira T, Rauvala H. 2002. Role of heparin-binding growth-associated molecule (HB-GAM) in hippocampal LTP and spatial learning revealed by studies on overexpressing and knockout mice. Mol Cell Neurosci. 20:330–342.

Place R, Lykken C, Beer Z, Suh J, McHugh TJ, Tonegawa S, Eichenbaum H, Sauvage MM. 2012. NMDA signaling in CA1 mediates selectively the spatial component of episodic memory. Learn Mem. 19:164–169.

Rasband MN. 2010. The axon initial segment and the maintenance of neuronal polarity. Nat Rev Neurosci. 11:552–562.

Sarrazin S, Lamanna WC, Esko JD. 2011. Heparan sulfate proteoglycans. Cold Spring Harb Perspect Biol. 3:a004952.

Scott RS, Henneberger C, Padmashri R, Anders S, Jensen TP, Rusakov DA. 2014. Neuronal adaptation involves rapid expansion of the action potential initiation site. Nat Commun. 5:3817.

Seidenbecher T, Laxmi TR, Stork O, Pape H-C. 2003. Amygdalar and hippocampal theta rhythm synchronization during fear memory retrieval. Science. 301:846–850.

Senkov O, Andjus P, Radenovic L, Soriano E, Dityatev A. 2014. Chapter 3 – Neural ECM molecules in synaptic plasticity, learning, and memory. In: Dityatev A, Wehrle-Haller B, Pitkänen A, editors. Progress in brain research. Brain

extracellular matrix in health and disease. Amsterdam, Netherlands: Elsevier. p. 53–80.

Senkov O, Mironov A, Dityatev A. 2015. A novel versatile hybrid infusion-multielectrode recording (HIME) system for acute drug delivery and multisite acquisition of neuronal activity in freely moving mice. Front Neurosci. 9:425. doi: 10.3389/fnins.2015.00425.

Shee WL, Ong WY, Lim TM. 1998. Distribution of perlecan in mouse hippocampus following intracerebroventricular kainate injections. Brain Res. 799:292–300.

Si W, Zhang X, Niu Y, Yu H, Lei X, Chen H, Cao X. 2010. A novel derivative of xanomeline improves fear cognition in aged mice. Neurosci Lett. 473:115–119.

Srinivasan J, Schachner M, Catterall WA. 1998. Interaction of voltage-gated sodium channels with the extracellular matrix molecules tenascin-C and tenascin-R. Proc Natl Acad Sci USA. 95:15753–15757.

Tendler A, Wagner S. 2015. Different types of theta rhythmicity are induced by social and fearful stimuli in a network associated with social memory. eLife. 4:e03614.

Vandecasteele M, Varga V, Berényi A, Papp E, Barthó P, Venance L, Freund TF, Buzsáki G. 2014. Optogenetic activation of septal cholinergic neurons suppresses sharp wave ripples and enhances theta oscillations in the hippocampus. Proc Natl Acad Sci. 111:13535–13540.

Yamaguchi Y, Inatani M, Matsumoto Y, Ogawa J, Irie F. 2010. Roles of heparan sulfate in mammalian brain development: current views based on the findings from Ext1 conditional knockout studies. In: Zhang L, editor. Progress in molecular biology and translational science. Glycosaminoglycans in development, health and disease. Cambridge, Massachusetts: Academic Press. p. 133–152.

Yoshimura T, Rasband MN. 2014. Axon initial segments: diverse and dynamic neuronal compartments. Curr Opin Neurobiol. 27C:96–102.

Zheng K, Bard L, Reynolds JP, King C, Jensen TP, Gourine AV, Rusakov DA. 2015. Time-resolved imaging reveals heterogeneous landscapes of nanomolar Ca(2+) in neurons and astroglia. Neuron. 88:277–288.